HEMT-Based Readout Technique for Dark- and Photon-Count Studies in NbN Superconducting Single-Photon Detectors

Jennifer Kitaygorsky, Sander Dorenbos, Elisabeth Reiger, Raymond Schouten, Val Zwiller, and Roman Sobolewski

***Abstract*—Dark counts in superconducting single-photon detectors (SSPDs) manifest themselves as spontaneous, transient voltage pulses, typically indistinguishable from photon counts. We present here a new readout technique based on integrating the SSPD with a low-noise, cryogenic high-electron-mobility transistor (HEMT) with high-input impedance. This arrangement allowed us to achieve amplitude resolution of the recorded output transients. In two-dimensional superconducting nanostripes, the physics of photon counting is based on the hotspot formation mechanism, while the dark counts correspond to voltage transients triggered by the vortex-antivortex motion and/or phase-slip centers. Thus, their respective transients can be distinguished by comparing the output pulse amplitude distributions. Our scheme also allowed us to perform photon-energy-resolution studies by comparing the SSPD output pulse amplitude distributions (the mean pulse amplitude and the distribution width) collected for incident single photons with different energies.**

***Index Terms*—Dark counts, photon-number resolution, photon spectral resolution, superconducting nanowires, superconducting single-photon detectors.**

I. Introduction

SUPERCONDUCTING single-photon detectors (SSPDs) are fast and reliable photon counters, which consist of a narrow (∼100 nm), ultrathin (4 nm), and long (∼0.5 mm) NbN stripe arranged in a meander structure, and are sensitive to photons from ultraviolet (UV) to near-infrared (NIR), with moderate quantum efficiency (QE), fast counting rates (>250 MHz), and very low dark counts and timing jitter [1]–[4].

The SSPD photoresponse is based on hotspot formation and supercurrent redistribution in a constricted volume of a superconducting nanostripe. The stripe is maintained at a temperature far below its critical temperature $T_{\rm c}$ and biased with a dc current $I_{\rm b}$ just below the critical current $I_{\rm c}$. After a photon of energy $h\nu \gg 2\Delta$ (where 2Δ is the superconductor energy gap) is absorbed, it breaks a Cooper pair, generating a highly excited quasiparticle (QP), which, through a cascade of electron-electron and electron-phonon interactions, leads to a large number of QPs with energies just above 2Δ, spatially forming in the stripe a local hotspot region of suppressed superconductivity [5].

Next, the hotspot expands, forcing $I_{\rm b}$ to be expelled from its volume toward the stripe edges or "sidewalks." When the supercurrent density in the sidewalks exceeds the critical value, superconductivity is destroyed across the width of the stripe and a resistive region is formed. This resistive region gives rise to a voltage signal. In the next thermal phase, the hotspot continues to grow due to Joule heating, forcing $I_{\rm b}$ flowing through the SSPD to drop and redistribute into the read-out circuit. This current redistribution allows the resistive region to decrease due to the QP recombination and out-diffusion. Eventually, the hotspot collapses, the superconductivity in the entire stripe is restored, and the detector is ready to register another photon. We note that the presented mechanism can lead to a macroscopic voltage signal only in nanostructured superconducting stripes that have a thickness smaller than and a width comparable with the initial hotspot dimensions.

The hotspot resistance $R_{\rm hs}$ can be estimated to be of the order of several hundred ohms to several kilo-ohms [6], depending on operating conditions and the SSPD $I_{\rm c}$. In most of the SSPD experiments performed to date, $I_{\rm b}$ redistributes to the $R_{\rm L} = 50\ \Omega$ load impedance (typically, the characteristic impedance of an output coaxial line); thus, the amplitude of the observed response is simply given by $V_{\rm pulse} \approx G \times (I_{\rm b} - I_{\rm ret}) \times 50\ \Omega$, where G is the amplifier gain [7], [8] and $I_{\rm ret}$ is the value of current flowing through the device at the highest value of $R_{\rm hs}$. The speed of $I_{\rm b}$ redistribution determines, in turn, the SSPD response pulse width and is limited by the superconducting meander kinetic inductance $L_{\rm k}$. Thus, in a conventional SSPD readout, when the device is connected directly to the output transmission line, the amplitude and the shape of the detected voltage pulse are simply determined by $I_{\rm b}$ and $L_{\rm k}$, irrespectively of the actual physics of photoresponse or dark-count mechanism. The response signal is also insensitive to the actual number of photons incident on the device, or their energy.

Reference [9] first proposed that, in principle, if we place an amplifier with a high load impedance next to the SSPD, such that $R_{\rm L} > R_{\rm hs}$, it should be possible to read out the true amplitude of the voltage pulses, and in turn $R_{\rm hs}$, such that $V_{\rm pulse} \approx G \times (I_{\rm b} -$

Manuscript received August 26, 2008. First published June 30, 2009; current version published July 10, 2009. This work was supported in part by the US AFOSR Grant FA9550-6-1-0348.

J. Kitaygorsky was with the University of Rochester, Rochester, NY 14627 USA. She is now with the Electromagnetic Applications in Lakewood, CO USA.

S. Dorenbos, R. Schouten, and V. Zwiller are with the Quantum Transport Group at Delft University of Technology, 2628 CJ Delft, The Netherlands.

E. Reiger was with the Delft University of Technology, 2628 CJ Delft, The Netherlands. She is now with the Universität Regensburg, D-93040 Regensburg, Germany.

R. Sobolewski is with the Department of Electrical and Computer Engineering, University of Rochester, Rochester, NY 14627-0231 USA (e-mail: roman.sobolewski@rochester.edu).

Digital Object Identifier 10.1109/TASC.2009.2018191

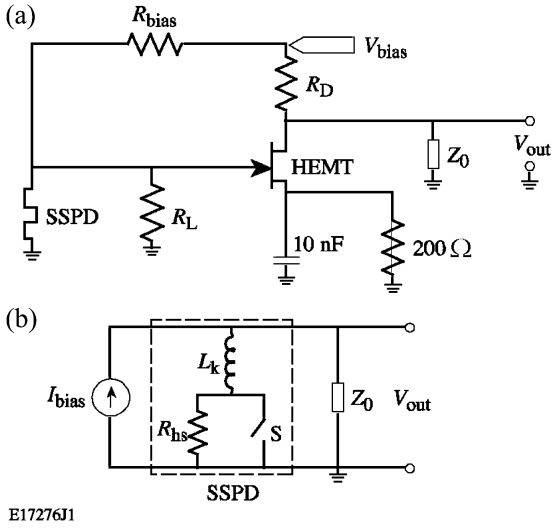

Fig. 1. (a) Circuit schematics implementing HEMT amplifier and 500-Ω load resistor $R_{\rm L}$. The 10-nF capacitor sets the maximum ac gain and a 200-Ω resistor sets the dc current for the HEMT; $R_{\rm bias}$ and $R_{\rm D}$ are the biasing and pull-up resistors, respectively. (b) Standard electrical photoresponse model of the SSPD with S denoting the detector switching action. $Z_0 = 50\ \Omega$.

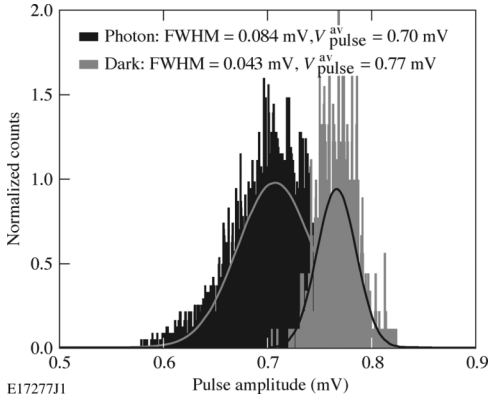

Fig. 2. Pulse-amplitude histograms of dark counts (red) and photon counts at $\lambda = 700$ nm in the single-photon regime (black). Measurements were performed at 4.2 K and at $I_{\rm b} = 0.8\ I_{\rm c}$. The SSPD output voltage amplitudes are divided by the amplifier gain.

$I_{\rm ret}) \times R_{\rm hs}$. Such an approach should enable us to distinguish the difference between the dark and photon counts, by looking at pulse amplitudes directly, and even achieve the spectral and photon-number resolution.

In this work, we present a new readout technique, which utilizes a high-electron-mobility transistor (HEMT) directly, *in-situ*, integrated with the SSPD, in order to achieve output pulse amplitude resolution. Because HEMT input impedance is nearly infinite, we have also implemented $R_{\rm L} = 500\ \Omega$ in parallel with our SSPD.

II. Experimental Setup

NbN films were deposited by dc reactive magnetron sputtering onto sapphire substrates at 900 K [10], resulting in epitaxial-quality films, and patterned by e-beam lithography and reactive-ion etching [11]. The device used in this work was characterized by $T_{\rm c} \approx 10$ K, normal sheet resistance $R_{\rm s} \approx 900\ \Omega$/square at $T = 20$ K, $L_{\rm k} \approx 600$ nH, $I_{\rm c} = 5.6\ \mu$A at $T = 4.2$ K, and QE $= 2\%$ for photons with wavelength $\lambda = 700$ nm.

A schematic of the HEMT-based readout circuit is shown in Fig. 1(a), together with the standard SSPD operation equivalent circuit [Fig. 1(b)]. The SSPD was mounted (wire-bonded) on the same printed circuit board as the HEMT and $R_{\rm L}$, and the entire circuit was placed inside a liquid-helium cryostat. The HEMT acts as an infinite-impedance element to separate the 50-Ω output transmission line from the SSPD. Because the HEMT input impedance is very high, we also utilize a 500-Ω load (or shunt) resistor $R_{\rm L}$ in parallel with the detector and the HEMT, as is shown in Fig. 1(a). The output electrical connections were achieved through a 50-Ω coaxial cable and a 0.08- to 26-GHz-bandwidth custom-made bias-tee. Such an integrated arrangement allowed us to dc bias both the SSPD and HEMT, using $R_{\rm bias} = 150\ {\rm k}\Omega$, mounted on the board together with the rest of the components, and, simultaneously, read out the ac photoresponse voltage signal. By applying the detector transient response to the gate of the HEMT, we can read out the drain voltage, which should, for $R_{\rm L} \gg R_{\rm hs}$, be proportional to the hotspot resistance and equal to $V_{\rm out}$. The $V_{\rm out}$ signal, constituting either the photon- or dark-count event, is read out using a 0.01- to 8.5-GHz-bandwidth amplifier and a 6-GHz single-shot oscilloscope. As a photon source, we used a tunable Ti:sapphire modelocked laser or a NIR laser diode, heavily attenuated and fiber coupled to our SSPD. For dark-count measurements, the detector was blocked from all incoming radiation, i.e., shielded inside the cryostat by a metallic enclosure.

To understand the electrical photoresponse of our SSPDs and decide on the operating parameters of the readout circuit, we have performed extensive circuit simulations using the SSPD-equivalent circuit shown in Fig. 1(b) and a commercial PSpice program [12]. The PSpice simulations revealed that $R_{\rm L}$ values higher than $\sim 270\ \Omega$ lead to an underdamped circuit, due to a small parasitic capacitance coming from a circuit board, as well as other components, estimated to be around 2 to 3 pF, and, eventually, to latching. Thus, we choose the value of $R_{\rm L}$ to be 500 Ω as a trade-off for having the highest $R_{\rm L}$ possible with a limited amount of underdamping and no latching, even though we realized that this value was going to be lower than the $R_{\rm hs}$ formed in our SSPD and estimated to be $\sim 1.2\ {\rm k}\Omega$. Thus, the $V_{\rm out}$ signals we are presenting in this work are actually proportional to a parallel connection of R_L and $R_{\rm hs}$, limiting our ability to fully, quantitatively distinguish between the different types of the SSPD counting events. Thus, our experimental observations are mainly qualitative.

III. Experimental Results

A. Dark-Count Versus Photon-Count Events

Fig. 2 presents histograms that compare pulse-amplitude distributions of the dark- (gray) and photon-count (black) events. The photon counts were collected for a very weak illumination (i.e., average number of absorbed photons per pulse $n \ll 1$) from a Ti:sapphire laser operating at $\lambda = 700$ nm. The amplitude histograms were very accurately fit with Gaussian distributions (solid lines). We can clearly see that the HEMT readout

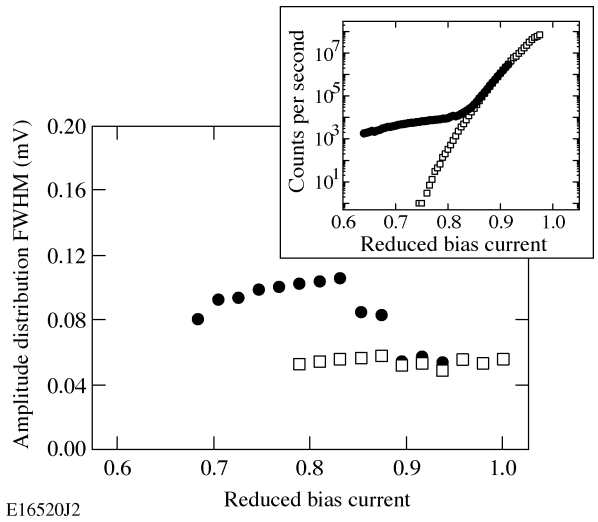

Fig. 3. Amplitude distribution width (FWHM of Gaussian fits) for dark counts (open squares) and photon counts such that $n \ll 1$ (closed circles). The inset shows the counting rate as a function of bias current for dark counts (open squares) and photon counts with $n \ll 1$ (closed circles).

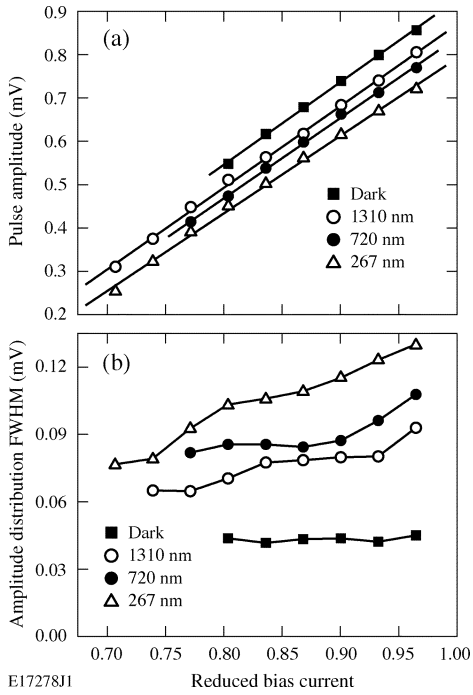

Fig. 4. Comparison of (a) mean-pulse amplitudes and (b) FWHM as a function of the SSPD normalized bias current for 267-nm photons (open triangles), 720-nm photons (closed circles), 1310-nm photons (open circles), and dark counts (closed squares).

allows us to easily distinguish between the dark and photon counts, as the average voltage $V_{\rm pulse}^{\rm av}$ of the dark-count pulses is substantially larger than in the case of photon pulses. Correspondingly, the full-width-at-half-maximum (FWHM) distribution of the Gaussian fit for dark-count events is twice as narrow as the photon-count-pulse FWHM. The latter is also illustrated in Fig. 3, which presents the FWHMs of the dark- and photon-pulse amplitude distributions at different $I_{\rm b}$'s. We note that the dark-count FWHM (open squares) is independent of $I_{\rm b}$, while for photon counts in the $n \ll 1$ regime (closed circles), as $I_{\rm b}$ approaches $I_{\rm c}$, the FWHM starts to drop around $I_{\rm b} = 0.83\, I_{\rm c}$. In this range, the dark counts simply start to dominate over the photon counts and, eventually, both FWHMs overlap at $I_{\rm b} > 0.9\, I_{\rm c}$. The latter behavior agrees very well with our earlier observation of the dependence of photon- and dark-count rates on $I_{\rm b}/I_{\rm c}$, as shown in the inset in Fig. 3.

The behavior shown in Figs. 2 and 3 can be explained as follows: because the fabrication of SSPDs is not perfect, we know that there must be a variation in width and, likely (due to, e.g., substrate imperfections and/or local defects), in thickness of our NbN stripes [13]. We also know that the experimental $I_{\rm c}$ is determined by the narrowest and thinnest section(s) of the stripe. The dark counts are most likely to be generated in these particular sections because, as we have demonstrated before [14], [15], they are due to either phase-slip centers or vortex-antivortex pair unbinding in our NbN stripes, depending on the stripe geometry and properties. As the dark counts originate at the weakest constriction sites of the SSPD meander, the Joule heating resulting from the events produces a normal region that is going to have only slight variations in resistance and an averaged value expected to be the largest (narrowest constriction). On the contrary, hotspot-driven photon-count events can be triggered, in principle, at any place along the length and the width of the meander, naturally leading to variations in collected voltage pulses and resulting in the overall broadening of the pulse-amplitude distribution with somewhat lower mean peak value. The latter effect will be amplified by any fluctuations in the meander width, as they translate to fluctuations of final hotspot resistance. In summary, in case of an SSPD with a perfect NbN meander (no constrictions), we expect a large number of photon counts and large QE [13], with almost negligible dark counts.

B. Photon Energy Resolution

We have also used the HEMT readout setup to perform studies on the SSPD capability to resolve the energy of incident photons. In our previous study [11], we have already demonstrated that SSPDs are suitable for photon-energy-resolved measurements. We have developed a statistical approach, based on the well-documented fact that QE of SSPDs very strongly (quasi-exponentially) depends on the photon wavelength and the normalized current biasing [16]. Thus, by measuring the SSPD system QE at different $I_{\rm b}$'s, we were able to resolve λ of the incident photons with a resolution of 50 nm. Here our approach is going to relate the average output pulse amplitudes and their FWHM to the energy of detected photons.

As a light source, we used a laser diode with $\lambda = 1310\ {\rm nm}$ and a Ti:sapphire with a frequency-tripling system to, overall, illuminate our SSPD with three different photon wavelengths (267 nm, 720 nm, and 1310 nm) and to compare its photoresponse. The obtained amplitude histograms in each case, as well as that for dark counts, were fit again with Gaussian distributions and studied in detail at different laser intensities and bias currents. The results presented in Fig. 4 demonstrate that, indeed, we were able to observe clear differences in both $V_{\rm pulse}^{\rm av}$ and FWHMs between the dark counts and the three aforementioned photon wavelengths.

Fig. 4(a) shows a plot of the mean-pulse amplitudes as a function of $I_{\rm b}$ in the single-photon regime for the three different photon wavelengths plus the dark counts. As expected, the averaged $V_{\rm pulse}^{\rm av}$ increases linearly with the $I_{\rm b}$ increase, but now we can also see that the pulse amplitude increases with the photon-wavelength increase (decreases with the photon-energy increase), with the dark counts having the highest amplitude.

Fig. 4(b) presents the FWHM values of the same histogram distributions of photon and dark counts used to compound Fig. 4(a). We note that the FWHM increases with the photon-energy increase (decreases with the photon-wavelength increase), which is logical given that the higher-energy photons can break more Cooper pairs, meaning they can readily activate more stripe sections along the NbN meander, especially when $I_{\rm b}$ approaches $I_{\rm c}$. As a result, for photons with the highest energies, we observe the widest FWHM of the distribution with the smallest $V_{\rm pulse}^{\rm av}$ [see Fig. 4(a)]. The lower-energy photons, on the other hand, can activate only the narrowest stripe segments, where the local, normal-state resistance should be the highest. Thus, for NIR photons, on average, we observe more-uniform output pulses (narrow FWHM) with the largest $V_{\rm pulse}^{\rm av}$ [see Fig. 4(a)].

The overall behavior presented in Fig. 4 is consistent with the earlier observation reported in [17]; our interpretation is, however, more conservative. Given the above data, we feel that it is more likely that the differences in the amplitude distributions observed in output transients of the SSPD illuminated by photons of different energies stem from local nonuniformities of the SSPD meander, instead of being caused by a true, intrinsic spectral resolution of a photon-excited superconducting nanowire.

IV. Conclusion

We have implemented a HEMT-based, high-load readout setup that allowed us to resolve the amplitude variations of the SSPD output transients, when the device was either illuminated with photons of different energies or completely isolated and generated the dark counts only. Using the HEMT setup, despite its limitation (namely, that we could not fulfill the $R_L > R_{\rm hs}$ condition) we could, nevertheless, with the good contrast, qualitatively distinguish the signals coming from either photon counts or dark counts, confirming that the physical origins of both events are different. The observed, readout-enhanced sensitivity of our output transients to variations in $R_{\rm hs}$ coming from illumination of the same SSPD with single photons of different energies is very encouraging, since it can be the basis for an easy and efficient determination of the energy of unknown incoming photons intercepted by the SSPD (using, e.g., an earlier pre-calibrated detector). As we stressed before, the presented here HEMT readout has some practical limitations. Ideally, we want $R_{\rm L} \gg R_{\rm hs}$ to achieve fully quantitative spectral resolution and, in consequence, the photon-number resolution. In our design, the increase of $R_{\rm L}$ beyond 500 Ω has, unfortunately, led to the HEMT circuit underdamped oscillations and even latching of SSPDs. Thus, further circuit design investigations and a more advanced, possibly amplifier-type, approach are needed to fully succeed with this SSPD output signal amplitude-resolving integrated high-input-impedance readout circuitry.

Acknowledgment

The authors thank Prof. Gol'tsman's group from the Moscow State Pedagogical University for the high-quality NbN films and also Prof. Hans Mooij from the Delft University of Technology for very valuable discussions.

References

[1] G. N. Gol'tsman, O. Okunev, G. Chulkova, A. Lipatov, A. Semenov, K. Smirnov, B. Voronov, A. Dzardanov, C. Williams, and R. Sobolewski, "Picosecond superconducting single-photon optical detector," *Appl. Phys. Lett.*, vol. 79, pp. 705–707, 2001.

[2] R. Sobolewski, A. Verevkin, G. N. Gol'tsman, A. Lipatov, and K. Wilsher, "Ultrafast superconducting single-photon optical detectors and their applications," *IEEE Trans. Appl. Supercond.*, vol. 13, pp. 1151–1157, 2003.

[3] W. Słysz, M. Węgrzecki, J. Bar, P. Grabiec, M. Górska, V. Zwiller, C. Latta, P. Böhi, A. J. Pearlman, A. S. Cross, D. Pan, J. Kitaygorsky, I. Komissarov, A. Verevkin, I. Milostnaya, A. Korneev, O. Minayeva, G. Chulkova, K. Smirnov, B. Voronov, G. N. Gol'tsman, and R. Sobolewski, "Fibre-coupled, single photon detector based on NbN superconducting nanostructures for quantum communications," *J. Mod. Opt.*, vol. 54, pp. 315–326, 2007.

[4] J. Zhang, W. Słysz, A. Verevkin, O. Okunev, G. Chulkova, A. Korneev, A. Lipatov, G. N. Gol'tsman, and R. Sobolewski, "Response time characterization of NbN superconducting single-photon detectors," *IEEE Trans. Appl. Supercond.*, vol. 13, pp. 180–183, 2003.

[5] A. D. Semenov, G. N. Gol'tsman, and A. A. Korneev, "Quantum detection by current carrying superconducting film," *Physica C*, vol. 351, pp. 349–356, 2001.

[6] J. K. W. Yang, A. J. Kerman, E. A. Dauler, V. Anant, K. M. Rosfjord, and K. K. Berggren, "Modeling the electrical and thermal response of superconducting nanowire single-photon detectors," *IEEE Trans. Appl. Supercond.*, vol. 17, pp. 581–585, 2007.

[7] A. J. Kerman, E. A. Dauler, W. E. Keicher, J. K. W. Yang, K. K. Berggren, G. Gol'tsman, and B. Voronov, "Kinetic-inductance-limited reset time of superconducting nanowire photon counters," *Appl. Phys. Lett.*, vol. 88, p. 111116, 2006.

[8] R. H. Hadfield, A. J. Miller, S. W. Nam, R. L. Kautz, and R. E. Schwall, "Low-frequency phase locking in high-inductance superconducting nanowires," *Appl. Phys. Lett.*, vol. 87, p. 203505, 2005.

[9] M. G. Bell, A. Antipov, B. Karasik, A. Sergeev, V. Mitin, and A. Verevkin, "Photon number-resolved detection with sequentially connected nanowires," *IEEE Trans. Appl. Supercond.*, vol. 17, pp. 289–292, 2007.

[10] G. N. Gol'tsman, K. Smirnov, P. Kouminov, B. Voronov, N. Kaurova, V. Drakinsky, J. Zhang, A. Verevkin, and R. Sobolewski, "Fabrication of nanostructured superconducting single-photon detectors," *IEEE Trans. Appl. Supercond.*, vol. 13, pp. 192–195, 2003.

[11] E. Reiger, S. Dorenbos, V. Zwiller, A. Korneev, G. Chulkova, I. Milostnaya, O. Minaeva, G. Gol'tsman, J. Kitaygorsky, D. Pan, W. Słysz, A. Jukna, and R. Sobolewski, "Spectroscopy with nanosctructured superconducting single photon detectors," *IEEE J. Sel. Top. Quantum Electron.*, vol. 13, pp. 934–943, 2007.

[12] Cadence. San Jose, CA, 95134 [Online]. Available: http://www.cadence.com

[13] A. J. Kerman, E. A. Dauler, J. K. W. Yang, K. M. Rosfjord, V. Anant, K. K. Berggren, G. N. Gol'tsman, and B. M. Voronov, "Constriction-limited detection efficiency of superconducting nanowire single-photon detectors," *Appl. Phys. Lett.*, vol. 90, p. 101110, 2007.

[14] J. Kitaygorsky, J. Zhang, A. Verevkin, A. Sergeev, A. Korneev, V. Matvienko, P. Kouminov, K. Smirnov, B. Voronov, G. Gol'tsman, and R. Sobolewski, "Origin of dark counts in nanostructured NbN single-photon detectors," *IEEE Trans. Appl. Supercond.*, vol. 15, pp. 545–548, 2005.

[15] J. Kitaygorsky, I. Komissarov, A. Jukna, D. Pan, O. Minaeva, N. Kaurova, A. Divochiy, A. Korneev, M. Tarkhov, B. Voronov, I. Milostnaya, G. Gol'tsman, and R. Sobolewski, "Dark counts in nanostructured NbN superconducting single-photon detectors and bridges," *IEEE Trans. Appl. Supercond.*, vol. 17, pp. 275–278, 2007.

[16] A. Korneev, P. Kouminov, V. Matvienko, G. Chulkova, K. Smirnov, B. Voronov, G. N. Gol'tsman, M. Currie, W. Lo, K. Wilsher, J. Zhang, W. Słysz, A. Pearlman, A. Verevkin, and R. Sobolewski, "Sensitivity and gigahertz counting performance of NbN superconducting single-photon detectors," *Appl. Phys. Lett.*, vol. 84, pp. 5338–5340, 2004.

[17] P. Haas, A. Semenov, H.-W. Hübers, J. Beyer, A. Kirste, T. Schurig, K. Il'in, M. Siegel, A. Engel, and A. Smirnov, "Spectral sensitivity and spectral resolution of superconducting single-photon detectors," *IEEE Trans. Appl. Supercond.*, vol. 17, pp. 298–301, 2007.